Interaction of amphiphilic nanoparticles with structurally perturbed lipid membranes

by

Alexander Derry

Submitted to the
Department of Materials Science and Engineering
in partial fulfillment of the requirements for the degree of

Bachelor of Science

at the

Massachusetts Institute of Technology

May 2018

Signature of Author.....
Department of Materials Science and Engineering
May 4, 2018

Certified by.....
Alfredo Alexander-Katz
Associate Professor of Materials Science and Engineering

Accepted by.....
Juejun Hu
Associate Professor of Materials Science and Engineering
Chairman, Undergraduate Committee

Interaction of amphiphilic nanoparticles with structurally perturbed lipid membranes

by
Alexander Derry

Submitted to the Department of Materials Science and Engineering
on May 4, 2018 in partial fulfillment of the
requirements for the degree of Bachelor of Science in
Materials Science and Engineering

Abstract

Understanding the interactions between nanoparticles and lipid membranes is important for applications such as drug delivery and membrane-protein mimetics. Perturbations such as area asymmetry and lateral tension affect these interactions by inducing various structural changes to the membranes. We use molecular dynamics simulations to demonstrate that the introduction of area asymmetry to a bilayer membrane significantly decreases the insertion latency of amphiphilic gold nanoparticles into both the densely and sparsely packed leaflets. We further demonstrate using transition state analysis that the dominant mechanisms for insertion into the dense and sparse leaflets are lipid desorption and lipid tail protrusions, respectively. These findings are supported by potential of mean force calculations showing that the energy barrier to protrusion is lower in the sparse leaflet, while that of desorption is lower in the dense leaflet. We also demonstrate that the structural characteristics of the bilayer when subject to lateral tension are similar to that observed in membranes with area asymmetry, suggesting a similar reduction in insertion latency. Further, we observe that lateral tension also increases the likelihood of nanoparticle ligands flipping across the bilayer, which is necessary for the nanoparticle adopting a stable symmetric configuration in the membrane.

Acknowledgements

I would like to thank Mukarram Tahir, my mentor throughout this project, for his guidance and support. His computational expertise and tireless work in planning, analysis, and debugging with me were invaluable, and without him this thesis would not be possible. He helped me become a much better researcher, and for that I am extremely grateful.

I would also like to thank Professor Alfredo Alexander-Katz for welcoming me into his lab and helping me get set up with my project.

Table of Contents

Abstract……...1

Acknowledgements……2

Table of Contents……... 4

List of Figures……5

1. Introduction……...5

1.1 Lipid bilayer membranes and transmembrane proteins…….. 6

1.2 Amphiphilic nanoparticles as biomimetic nanostructures……. 7

1.3 Pathways of uptake into lipid membranes……. 8

1.4 Area asymmetry in lipid membranes……... 10

1.5 Membranes under tension……... 11

2. Computational Methods……... 13

2.1 Molecular dynamics……13

2.2 System setup…….. 15

2.3 Analysis of bilayer defects……...19

2.4 Umbrella sampling and potential of mean force calculations……...20

2.5 Nanoparticle uptake simulations…….21

3. Results and Discussion……..23

3.1 Properties of symmetric and asymmetric bilayers……... 24

3.1.1 Structural characteristics……24

3.1.2 Frequency of protrusions and hydrophobic defects……26

3.1.3 Protrusion and desorption potential of mean force……27

3.2 Nanoparticle uptake behavior…….. 30

3.2.1 Insertion latency……30

3.2.2 Transition state analysis……33

3.3 Effect of tension on membrane-nanoparticle interactions……... 37

3.3.1 Bilayer structural characteristics……37

3.3.2 Membrane-nanoparticle interactions under tension……38

4. Conclusions and Future Work……40

5. References……42

List of Figures

Figure 1. Visualizations of elbow and splay lipid tail protrusions

Figure 2. Chemical structure and MD representations of DOPC

Figure 3. Chemical structure and MD representations of nanoparticle constituents

Figure 4. GROMOS and MARTINI representations of MUS:OT NPs with radial distribution function

Figure 5. Structural characteristics of asymmetric bilayer: snapshot, density profile, and deuterium order parameter

Figure 6. Area distribution of hydrophobic defects for sparse leaflet of asymmetric bilayer

Figure 7. Potential of mean force for splay protrusion in dense and sparse leaflets

Figure 8. Potential of mean force for lipid desorption in dense and sparse leaflets

Figure 9. Fraction of NPs inserted as a function of simulation time for asymmetric and symmetric bilayers

Figure 10. Committor (p) as a function of starting configuration time and snapshots of transition states for dense and sparse leaflets

Figure 11. Proposed generalized pathways for insertion into dense and sparse leaflets

Figure 12. Structural characteristics of bilayer under tension: snapshot, density profile, and deuterium order parameter

Figure 13. Membrane failure modes in bilayer with and without embedded NP

1. Introduction

1.1 Lipid bilayer membranes and transmembrane proteins

Lipid bilayer membranes are a critical component of all biological systems, forming the barrier between a cell and its external environment. Due to their amphiphilic nature, lipid molecules self-assemble into bilayers with the hydrophobic lipid tails segregated from the aqueous environment by the hydrophilic heads. The hydrophobic region in the core of the membrane results in a significant energy barrier (>20 kcal/mol) to the trans-membrane diffusion of polar and charged species, which are much more energetically stable in the presence of water [1], [2]. Due to this barrier, one of the key functions of the cell membrane is to control the transport of molecules into and out of the cell. This movement is tightly regulated by embedded membrane proteins which act as transport channels [3].

Transmembrane proteins are highly diverse and often quite complex in structure and function. Ion channels are a particular class of transmembrane proteins which regulate the transport of a specific small molecule (e.g. water, Cl^-, Na^+, K^+, or Ca^{2+}) into or out of the cell. The regulation is often highly selective, providing permeability to only a specific anion or cation; some channels are even able to distinguish between very similar ions such as K^+ and Na^+ [4]. Such channels can function by either allowing the ions to diffuse down their electrochemical gradient or by the activation of a gating mechanism by an external stimulus such as voltage, ligand binding, or membrane tension. Ion channels play an essential role in many biological functions, including the regulation of membrane potential, cell volume, and electrical signaling in the nervous system [4]–[6]. For this reason, ion channel dysfunction has been linked to diseases such as cystic fibrosis, epilepsy, cardiac arrhythmias, and even Alzheimer's disease [7]–[9]. In addition to channels, membrane proteins also play a role in membrane fusion, a process

that is crucial to biology because it drives processes such as viral endocytosis, intercellular transport of molecules in vesicles, and the secretion of neurotransmitters [10], [11]. Due to their biological importance, there is significant interest in engineering synthetic nanostructures that mimic the behavior of these complex transmembrane proteins.

1.2 Amphiphilic nanoparticles as biomimetic nanostructures

Nanoparticles (NPs) are the most promising materials for applications which require interaction with the cell membrane. In addition to their size and morphology being adjustable, the surface properties and chemistry of NPs can be tuned by functionalizing the surface with various ligands. This high tunability means that NPs are suitable for a wide range of biological applications. Drug delivery and imaging have become particularly important medical applications of NPs due to their potential for cellular uptake and targeted localization [12], [13]. Gold is most commonly used as a core material for biological NPs because it is non-toxic, easy to synthesize, and readily forms thiol linkages which enable functionalization with a wide variety of ligands [14]. Many particles designed for drug delivery, particularly those with a diameter of 10–100 nm, are internalized through endocytosis, whereby the cell membrane engulfs the particle and forms a vesicle around it as it enters the cell [15]. Small cationic gold NPs (AuNPs) can penetrate membranes without endocytosing, but they have been shown to induce pores and other defects which lead to membrane permeability and sometimes cell death [16]. However, NPs designed to mimic transmembrane proteins must enter and fuse with the cell membrane nondisruptively without causing poration, endocytosis, or cell death.

It has been shown experimentally and computationally that anionic, amphiphilic, monolayer-protected gold NPs with a diameter of less than 10 nm can spontaneously embed

themselves in lipid bilayer membranes [17]. These particles can be functionalized with a variety of sulfonate groups attached to the ends of alkanethiol ligands grafted to the gold core. The hydrophobic alkane chains enable membrane insertion through the hydrophobic effect, while the anionic sulfonate groups make the particle soluble in water. The structure of these NPs was modeled after amphiphilic membrane proteins, which can nondisruptively exist in membranes through a process known as "snorkeling", whereby their secondary structure significantly rearranges to position aliphatic sections in the hydrophobic bilayer core and charged residues in the polar interface region [18]. Through this mechanism, the free energy barrier to membrane translocation is significantly reduced, and thus amphiphilic NPs of analogous structure interact with membranes in a similar manner [19]. Additionally, once embedded these particles have been shown in simulations to impact the membrane in a manner that is very similar to that of transmembrane proteins, making them highly promising as biomimetic channel materials [20].

1.3 Pathways of uptake into lipid membranes

The efficient uptake of NPs into lipid membranes is an important factor in their application as functional particles for drug delivery, imaging, or biomimetic protein channels. Spontaneous insertion into lipid bilayers is dependent on the presence of membrane defects, which include lipid tail protrusions and hydrophobic packing defects. Studies have shown that hydrophobic lipid tails stochastically protrude beyond the head groups and into the solvent. These protrusions can be classified into two modes, elbow or splay, depending on the position of the protruding tail atom (near or far from the head group, respectively; see Fig. 1). Contact between protrusions of both types is known to be a critical step in membrane fusion through the formation of a lipid stalk [11]. Through a similar mechanism, a functionalized gold nanoparticle

can be drawn into the membrane if contact occurs between a spontaneous lipid tail protrusion and a nearby hydrophobic group of the AuNP monolayer [21], [22]. This contact significantly lowers the kinetic barrier to insertion and allows the particle to fuse with the membrane. The frequency of these protrusions is affected by factors such as membrane curvature, which increases the average number of protrusions per lipid almost 1.5-fold. The fraction of splay protrusions was also shown to increase with increasing curvature [11].

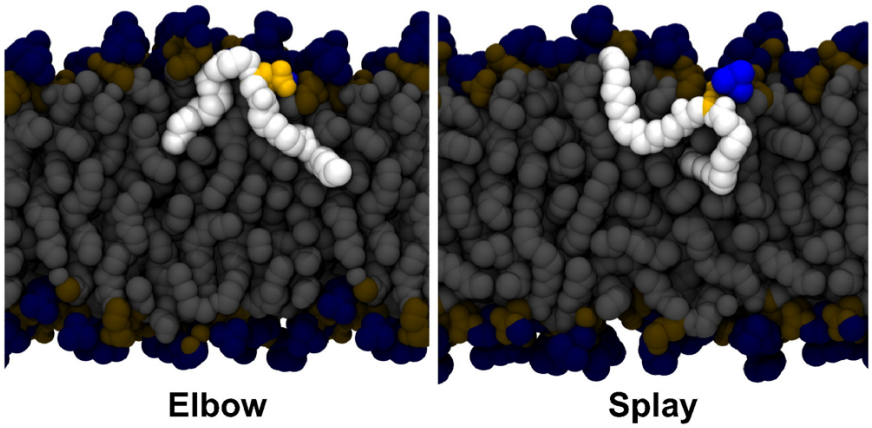

Figure 1. Visualizations of elbow and splay lipid tail protrusions, with the protruding tail in white and the phosphate of the protruding lipid in yellow. Figure from Tahir et al. [11].

Membrane curvature is also associated with lipid packing defects, which provide another potential pathway for particle insertion. Many peptides are able to adsorb to curved bilayer membranes due to the presence of a motif known as the Amphipathic Lipid Packing Sensor (ALPS) motif. ALPS motifs refer to a set of motifs consisting of larger hydrophobic residues interspersed between small polar, but mostly uncharged, residues. Like the amphipathic AuNPs discussed earlier, this makes them soluble in water but able to associate with membranes through the hydrophobic effect. These peptides can thus detect packing defects which increase the

surface area of accessible hydrophobic atoms [23]. Such defects have been shown to exist not only in curved membranes, but also in planar membranes containing lipids with a conical shape, which perturb the structure and properties of the bilayer [24]. Given that structural perturbations such as these are known to cause membrane defects which are associated with hydrophobic contact events, we can hypothesize that inducing such perturbations in membranes would accelerate the uptake of amphipathic nanoparticles.

1.4 Area asymmetry in lipid membranes

As discussed in the previous section, membrane curvature is an important factor in determining the frequency of bilayer defects and the ease of particle insertion. This is largely due to the nature of curved membranes, in which the positively curved leaflet (e.g. the outside leaflet of a vesicle) has a greater area per lipid (APL) than the negatively curved (inside) leaflet. This results in greater accessible space between head groups for protrusions to occur or for external ligands to contact the hydrophobic bilayer core. Indeed, there is some evidence that area asymmetry is associated with the uptake of some drugs and solutes, as well as viral fusion mediated by amphiphilic fusion peptides [25]. However, while the effects of membrane curvature have received significant attention, the detailed impact of area asymmetry on planar membranes in the context of bilayer defects and nanoparticle interactions is not well studied. Area asymmetry can be induced by other factors as well as curvature, such as asymmetric particle inclusions and obstructed lipid diffusion. Esteban-Martín et al. characterized the stability of asymmetric lipid distribution in membranes using a computational approach [26]. This study showed that lipid membranes are surprisingly stable over simulation time scales (tens of nanoseconds) even under high degrees of asymmetry (~60%). The leaflet with a greater number

of lipids compresses and deforms in an undulated manner, while that with fewer lipids expands and leaves solvated gaps between the heads. The tails of the lipids in the densely packed leaflet have a high order parameter and arrange perpendicular to the membrane normal, while the sparsely packed leaflet tends to thin out with spread and highly disorganized tails. Taken together, these results imply that area asymmetry in membranes could affect the incidence of defects such as packing defects and lipid tail protrusions, which in turn impacts the uptake of nanoparticles. Reducing NP insertion latency would have many benefits from an application standpoint. For one thing, the efficiency of NP delivery would improve because a greater fraction of particles administered would insert into membranes rather than desorbing into solution. Additionally, for targeted applications such as drug delivery or biosensing, it is often critical that the NP carrier reaches and adsorbs to its intended target quickly.

1.5 Membranes under tension

In addition to area asymmetry, membranes can be structurally perturbed by the application of mechanical force causing lateral membrane tension. Membrane tension plays a role in many cellular functions. For example, mechanosensitive channels, which sense forces and deformations in the surrounding bilayer, are important in how cells respond to events such as osmotic shock. When there is an imbalance in ion concentration between the interior of the cell and the extracellular environment, cells must adjust their osmolarity to prevent lysis due to high or low internal pressure. Specific channel proteins such as MscLs have been shown to protect against such shocks by allowing solutes and water in or out in response to changes in membrane tension [27], [28]. Due to their complexity, it is difficult to replicate these proteins with synthetic

peptides. However, given their biological importance, the development of NPs that can replicate their tension-dependent permeability properties would be highly valuable.

Simulation studies have shown that an applied pressure of -200 bar, regardless of loading rate, inevitably led to the formation of water pores and rupture of a pure lipid membrane [29]. Lai et al. showed that carbon nanoparticles with a fullerene structure can either increase or decrease the membrane's resistance to lateral tension depending on whether the particles were large or small, respectively [30]. Given the beneficial properties of amphiphilic AuNPs as membrane protein biomimetics, it is important to assess their interactions with lipid bilayers under tension in order to determine their potential as mechanosensitive channels.

This thesis uses computational simulations to investigate the interaction of amphiphilic AuNPs with lipid bilayers under structural perturbations, particularly area asymmetry and membrane tension. In order to test the hypothesis that NP insertion latency can be reduced by inducing area asymmetry in lipid bilayer membranes, we characterize planar membranes with various degrees of area asymmetry, assess the occurrence of relevant bilayer defects, and study the membrane's interactions with amphiphilic AuNPs. The properties of bilayers with embedded NPs and the probability of NP ligand flipping are also studied as a function of membrane tension. Taken together, this provides an assessment of the potential for amphiphilic AuNPs as biomimetic nanostructures to replace embedded transmembrane proteins or as vehicles for drug delivery and imaging applications.

2. Computational Methods

2.1 Molecular dynamics

Recently, computer simulations have become an indispensable tool in the study of biophysical systems due to the ability to perform analysis at an atomistic scale. Molecular dynamics (MD) is a simulation method for studying the evolution of a system of atoms and molecules over a fixed period of time. Due to the size and complexity of these systems (tens of thousands of atoms or more), it is impossible to analyze them analytically; therefore, MD numerically solves Newton's equations of motion to determine interactions between particles in the system [31]. The results of these simulations come in the form of large molecular trajectories, which describe the location and velocity of each particle in the system at each time-step.

In MD, the interactions between atoms and molecules are defined by force field parameterizations. The total potential energy of a molecular system includes the energy of bonded interactions (atoms connected by covalent bonds) and the energy of nonbonded interactions (long-range electrostatics and van der Waals bonds). This results in a force field energy of the following form:

$$E_{total} = E_{bonded} + E_{nonbonded} = (E_{bond} + E_{angle} + E_{dihedral}) + (E_{electrostatic} + E_{vdW}) \quad (1)$$

The interactions of atoms in a system can be parameterized based on these energy terms. For example, a force field may define bonded parameters such as bond stretching, bond angle bending, and dihedral angle bending and nonbonded parameters such as atomic mass, Coulomb potentials, and the C6/C12 terms of the Lennard-Jones potential [32], [33]. These parameterizations are empirical and vary depending on the specific atoms, molecules, and functional groups involved. Fully atomistic force fields define every atom in the system

separately for maximum resolution. United-atom models simplify this by grouping hydrogen atoms with heavy atoms into distinct beads (e.g. methyl groups). However, both of these types of models are computationally expensive and limits the possible system sizes and timescales; for this reason, coarse-grained (CG) force fields have also been developed to reduce the system's degrees of freedom by grouping atoms together into virtual "beads" [34].

In this research, all MD simulations were performed using the GROMACS open-source package, version 4.6.5 [35]. For atomistic simulations, the GROMOS 54a7 united-atom force field was used with the SPC water model [36]. Unless otherwise noted, all simulations used the NPT ensemble (fixed number of particles, pressure, and temperature; unit cell volume can change) with the following parameters. A leap-frog integrator with a time-step of 2 fs was used to integrate Newton's equations. The LINCS algorithm was used to solve bond constraints [37]. The fast smooth particle mesh Ewald (PME) method was used to model electrostatic interactions, with a Fourier grid spacing of 0.12 nm and fourth-order interpolation. The neighbor list, Coulomb, and van der Waals cutoffs were all 1.0 nm. Temperature was coupled at 310 K using a velocity-rescale thermostat with a time constant of 0.1 ps. Pressure was coupled at 1 bar using either a Berendsen or Parrinello-Rahman barostat with a time constant of 1.0 ps. Typically, the Berendsen barostat is used to efficiently scale the box at the beginning of a simulation run (equilibration), while the Parrinello-Rahman barostat is more accurate for data collection over longer time intervals. Pressure was coupled semi-isotropically so that box scaling was separate in the x/y and z dimensions, and the compressibility was set to 4.5×10^{-5} bar^{-1}. Periodic boundary conditions were used in all three dimensions. Coarse-grained simulations were modeled using the MARTINI force field, which combines four heavy atoms to a single bead. This allows for a larger time-step of 30 fs. Additionally, the neighbor list cut-off was increased to 1.4 nm, while

the Coulomb and van der Waals cutoffs were increased to 1.2 nm. The time constants for temperature and pressure coupling were 1 ps and 12 ps, respectively, and the compressibility was set to 3 x 10^{-4} bar^{-1}. Visual Molecular Dynamics (VMD) was used for all visualizations [38].

2.2 System setup

Atomistic simulations were based on a pre-equilibrated dioleoylphosphatidylcholine (DOPC) bilayer containing 128 lipids. DOPC is a phospholipid consisting of a positively charged choline head group, a negatively charged glycerophosphate group, and two unsaturated fatty acid tails. Atomistic and CG representations of the DOPC molecule are shown in Fig. 2. The bilayer lay in the x-y plane and was solvated with 45–50 water molecules per lipid. For simulations with a larger box size, the system was first replicated five times in the x and y directions using the Gromacs utility *genconf* and then cropped to the desired size using *editconf*. In most cases, the box size was cropped to 10 nm, corresponding to 244 lipids. This was primarily to allow enough space for the bilayer deformations caused by embedded NPs to dissipate before the box edge. For CG simulations, a bilayer of the desired size was created using the Python script insane.py, which can be found on the MARTINI website (http://www.cgmartini.nl/index.php/downloads/tools/239-insane).

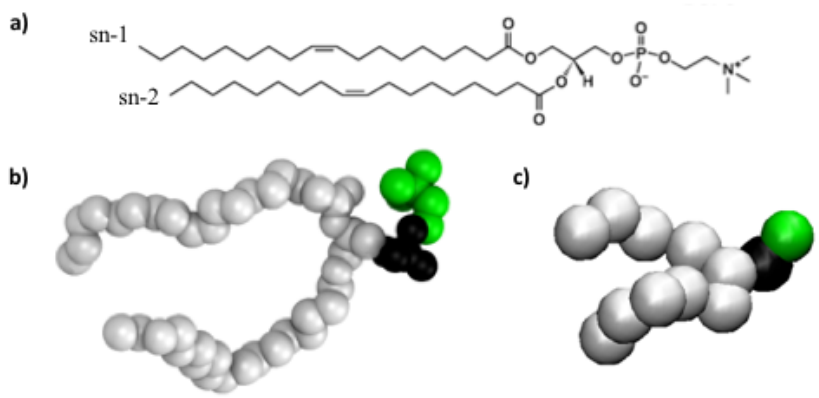

Figure 2. (a) Chemical structure of DOPC. (b–c) Simulation representations of DOPC in atomistic and coarse-grained resolution, respectively.

The nanoparticles used in this research were the monolayer-protected gold AuNPs shown by Van Lehn et al. to behave similarly to membrane proteins [20]. These consist of two ligand types: 11-mercapto-1-undecanesulfonae (MUS), consisting of 11 methylenes end-functionalized with a negatively charged sulfonate group, and octanethiol (OT), a simple hydrophobic chain of eight methylenes. The chemical structures and MD representations of all NP components are shown in Fig. 3. For tension studies, all-MUS NPs (58 ligands) were used, whereas 1:1 MUS:OT NPs (29 of each ligand) were chosen for insertion studies because the addition of hydrophobic OT ligands enhances uptake. All NPs had a gold core diameter of 2 nm.

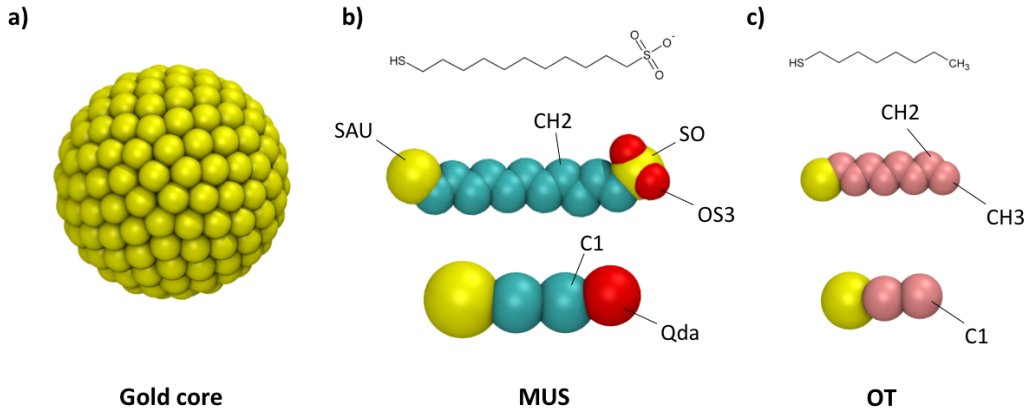

Figure 3. MD representations of (a) the gold core, (b) the MUS ligand, and (c) the OT ligand, with chemical structures also shown for both ligands. The gold core was 2 nm in diameter. All-MUS NPs consisted of 58 MUS ligands, while MUS:OT NPs consisted of 29 MUS and 29 OT ligands.

Figure 4 shows the atomistic and coarse-grained MD representations of MUS and MUS:OT NPs in water, as well as their radial distribution functions (RDFs) in GROMOS and MARTINI to demonstrate some of the differences between the two force fields. In the atomistic representation, the ligands are much more compact. This is due to the fact that the CG beads consist of 4 heavy atoms, restricting the bond angles and the degrees of freedom in the ligand carbon chains. The Na^+ RDF is also shifted outwards in the CG representation due to the less compact structure, while the NPs are solvated with water to about the same extent.

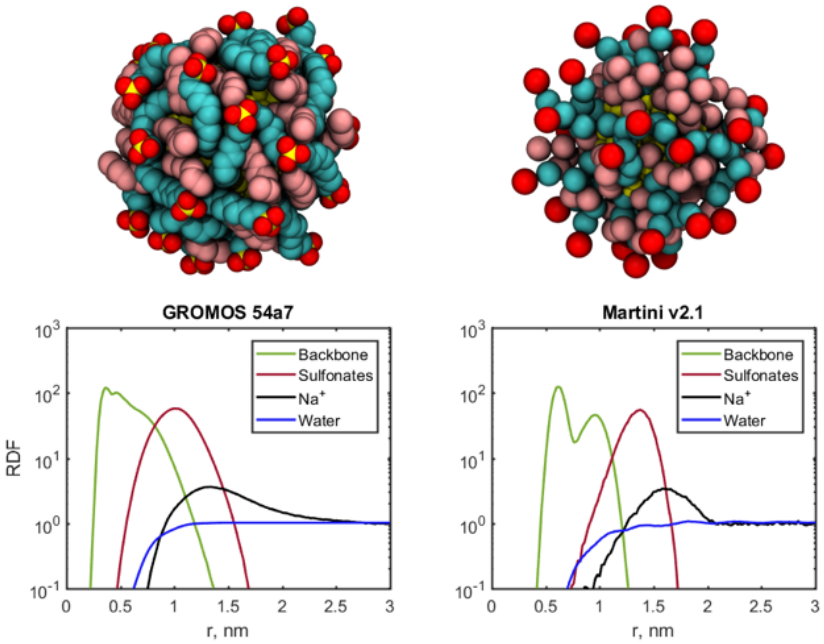

Figure 4. MUS:OT nanoparticle representations in GROMOS 54a7 (left) and MARTINI (right) force fields, as well as their RDFs with water and Na^+.

For ease of embedding in simulations with pre-embedded NPs, pre-configured NPs were used in which the ligands were split to either side by an applied force such that the charged MUS groups interact properly with the membrane. The Gromacs tool *g_membed* was used to embed the NPs by the following process. First, the NP was placed in the center of the bilayer and shrunk by 90% in the x/y dimensions. Then, any interfering lipids or solvent were removed before the NP was expanded back to its original size over 10,000 iterations. Due to the MUS NPs having a net negative charge, an appropriate number of NA^+ ions (58 for all-MUS and 29 for MUS:OT) were then added to the solvent to restore the system to neutral.

The asymmetric bilayer systems were set up by randomly removing lipids from the upper leaflet of the pre-equilibrated bilayer described above. The number of lipids in the upper leaflet was thus reduced by 5–40% in order to assess the impact of increasing area asymmetry on the

occurrence of bilayer defects and the uptake behavior of NPs. The lipids were all removed at once for simplicity even for asymmetries as high as 40%; it has been shown that this yields similar results to more gradual approaches [26].

The tension simulations were conducted by applying a uniform lateral pressure of -250 bar in the x-y plane while the pressure in the z-direction remained 1 bar (NP_zT). Tensed configurations were generated sequentially each time the box size increased by 0.2 nm. Starting from a fully equilibrated, untensed bilayer with a box size of 10 nm, tension was applied until the simulation failed due to box overcompression. From the resulting trajectory, the frame corresponding to the box size closest to 10.2 nm was extracted and equilibrated for 2 ns with box size fixed (NP_zAT). The equilibrated configuration was then pulled again, and the process was repeated until rupture. The equilibration between tension steps was necessary to allow the bilayer to expand without rupturing prematurely. For analysis of ligand flipping, a single NP was embedded in the membrane in the center of the box before applying tension.

2.3 Analysis of bilayer defects

Protrusions were defined based on the degree to which a lipid tail extended into the solvent. Previous studies have defined protrusions based on the distance between a tail atom and its corresponding phosphorous atom projected along the membrane normal. The threshold for considering a lipid tail protrusion was defined as $d_p > 0.1$ nm, as in previous studies [11]. Hydrophobic packing defects were calculated by projecting the lipid atoms of the leaflet in question onto a two-dimensional grid with spacing of 0.1 nm. At each grid position, the lipid atom with the greatest z-distance from the bilayer center (i.e. the first to be contacted from the solvent) was recorded. Contiguous patches in which a tail atom was the first contact were

considered hydrophobic defects, and the size of a patch was calculated based on the number of grid spaces it occupied. Unbiased CG simulations were run for 500 ns and the protrusion frequencies and defect area distributions were calculated from these trajectories for various degrees of membrane asymmetry. Both sparsely and densely packed leaflets were considered for all simulations.

2.4 Umbrella sampling and potential of mean force calculations

To assess the likelihood of events such as protrusion or desorption occurring, it is necessary to calculate the free energy barrier associated with the change in molecular configuration of the system. This is known as the potential of mean force (PMF), which is found by calculating the free energy profile along a defined reaction coordinate. The computation of a PMF requires each configuration along the reaction coordinate to be sampled, which may not be possible over simulation timescales due to the presence of energy barriers in the system making certain states practically inaccessible. This problem is mitigated through a method called umbrella sampling (US). In US, several biased simulations are performed in which the atom(s) of interest are constrained to a small window of space using a harmonic potential. This allows all states along the reaction coordinate to be sufficiently sampled (Roux 1994). After simulations have been run on sufficient configurations, the results are recombined to estimate the final PMF.

In this research, all PMFs were calculated in GROMOS using umbrella sampling and the Weighted Histogram Analysis Method (WHAM), which uses the overlapping energy distributions of the sampling windows to calculate the optimal, error-minimizing estimate of the unbiased distribution [39]. The bilayer normal (z-axis) was defined to be the reaction coordinate, and umbrella sampling was conducted with windows spaced by 0.1 nm. For both protrusion and

desorption, the bilayer normal was sampled to a maximum distance of 4.0 nm, for a total of 40 US windows each. For protrusions, the last bead of the sn-1 lipid tail was restrained, representing a splay protrusion, while for desorption the phosphate of the head group was restrained. For ligand flipping, the PMF was measured by restraining the sulfur of the sulfonate group on the MUS ligand at positions between -2.0 nm to 2.0 nm from the bilayer normal in the z-direction (41 US windows). The restrained beads were initially pulled to the desired position by a harmonic potential with a spring constant of 500 kJ/mol/nm^2 and restrained for 2 ns of equilibration before the spring constant was increased to 3000 KJ/mol/nm^2 for a further 70 ns of sampling. To determine how area asymmetry affects the energy barrier to protrusion or desorption, PMFs were calculated for each leaflet of an asymmetric bilayer with 25% lipid reduction in the upper leaflet. The ligand flipping PMF was calculated for a 276-lipid bilayer with and without lateral tension.

2.5 Nanoparticle uptake simulations

To assess the effect of bilayer asymmetry on the insertion latency of amphiphilic NPs, unbiased simulations were performed using MARTINI. Atomistic simulations were infeasible for this system due to the long timescales required for NP insertion (often on the order of microseconds). Here, a NP was placed in the solvent either above or below the bilayer such that the smallest distance between a NP ligand and a lipid atom was less than 1 nm. Four different systems were simulated: symmetric bilayer with NP above, symmetric bilayer with NP below, asymmetric bilayer (25% reduced) with NP above, and 25% reduced bilayer with NP below. Each asymmetric bilayer system was simulated 75 times, while each symmetric system was simulated only 50 times because the two leaflets are identical. Each simulation ran for either 100

microseconds or until the particle inserted or desorbed from the bilayer surface. The general pathway for the insertion of a NP into the planar face of a membrane involves the particle moving around on the surface of one leaflet for an extended time period before eventually it either (1) makes sufficient hydrophobic contact with a membrane defect (e.g., protrusion, desorption, packing defect) to be pulled into the membrane or (2) drifts away from the membrane into the body of solvent. A watchdog script monitored the number of hydrophobic contacts and distance to the bilayer throughout the simulation and terminated it if the number of contacts exceeded 10 (defining insertion) or the distance from the NP center of mass to the bilayer exceeded 9 nm (NP desorption). A hydrophobic contact was counted when two particles came within 0.6 nm of each other, and the time at which the number of hydrophobic contacts exceeded 10 was defined as the insertion latency. This threshold was chosen empirically based on the observed number required to permanently insert, since occasionally a NP would make a few contacts but fail to fully insert.

In order to determine the uptake mechanism for a NP once it had fully inserted, the transition state for insertion was identified using a process called committor analysis. The free-energy landscape of an NP in a bilayer system consists of two stable energy minima—the NP in solvent on the surface of the membrane (State A) and the NP fully inserted in the membrane (State B)—between which all configurations have a higher energy. The probability p that a simulation initiated at any of these intermediate configurations will end up in State A rather than State B is called the committor. Thus, the committor is equal to 1 if the NP starts embedded in the bilayer and is equal to 0 if the particle starts in the solvent. The transition state is defined as the configuration in which the system is equally likely to end up in State A as State B (i.e., $p = 0.5$), and lies at the

highest point of the free-energy curve between the two states (Du 1998). In this study, the committor for an inserted particle was calculated by extracting configurations every 90 ps in the 10-ns window around the NP insertion time, resulting in 112 configurations. The first several frames of this 10-ns trajectory correspond to states in which $p = 0$ and the last correspond to those in which $p = 1$; therefore, these configurations lie on the committor coordinate for insertion. For each initial configuration, p was calculated by running 10 unbiased simulations for 6 ns each, with randomly generated starting velocities for all particles, and recording how many particles committed to each state. This simulation time was considered more than sufficient to determine commitment based on previous studies [21]. Commitment to B (insertion) was determined if the number of hydrophobic contacts was greater than 10 at the end of the trajectory, while commitment to A was determined by less than 5 hydrophobic contacts. The transition state was considered to be the configuration nearest to $p = 0.5$.

3. Results and Discussion

3.1 Properties of symmetric and asymmetric bilayers

3.1.1 Structural characteristics

Asymmetry in APL between leaflets induces significant structural changes to the bilayer, which may in turn affect the incidence of membrane defects. Figure 5 shows the average density profile of the bilayer obtained from a 200-ns unbiased GROMOS simulation. Due to the lipids of the dense lower leaflet compressing and those of the sparse upper leaflet expanding as lipids were removed, the density profile of the bilayer became more asymmetric as the degree of area asymmetry increased. As such, the density of the upper leaflet significantly decreased while that of the lower leaflet increased slightly at an asymmetry of 25%. The decrease in density was also accompanied by a slight decrease in thickness of that leaflet. Note that many figures only show the difference between symmetric bilayers and bilayers with 25% asymmetry, even though simulations were run up to 40% symmetry for most systems. This was largely for clarity of visualization; in these cases, the relevant data changed monotonically with increasing area asymmetry. Moreover, 25% is larger than the degree of area asymmetry thought to be thermodynamically feasible in biological systems, with larger asymmetries likely representing metastable states [26].

The order parameter of the lipid tails was also analyzed for the same unbiased simulations. Order parameter is an important measure of orientational mobility of the acyl chains, which is strongly linked to the thermodynamic properties of the bilayer, including fluidity and permeability. Figure 5 also shows the deuterium order parameter ($S_{CD} = \frac{3<cos^2\theta - 1>}{2}$; θ is the time-dependent angle of the carbon-deuterium bond) as a function of the

carbon atom index in the acyl chain. A value of $S_{CD} = 0$ corresponds to a perfectly disordered state, while $S_{CD} = 0.5$ represents maximum order (all tails perfectly normal to the membrane plane with no mobility). As expected, the profile of the symmetric membrane shows that the order parameter of the two leaflets were approximately equal. The shape and value of the curve also agrees well with previous studies of lipid bilayers [40]. However, for the 25% asymmetric bilayer, the order parameter of the majority leaflet was significantly higher than that of the minority leaflet, with that of the symmetric leaflet falling in between. The degree to which the order parameter differed between the two leaflets increased as the carbon index increased (i.e. moving away from the head group), an effect which became more pronounced as the asymmetry increased. The magnitude of the difference also increased for all carbon indices as asymmetry increased. This is explained by the fact that the closely packed lipids of the majority leaflet become more constrained and thus lie mostly along the membrane normal, while the greater area (and volume) per lipid in the upper leaflet results in higher orientational disorder. This also helps explain the decrease in thickness of the lower-density leaflet, as more tails began lying perpendicular to the membrane normal, as shown in the snapshot on the left of Fig. 5. Considering that high lipid tail mobility is a prerequisite for protrusions, these data suggest that the likelihood of protrusions in the upper leaflet should increase as area asymmetry increases.

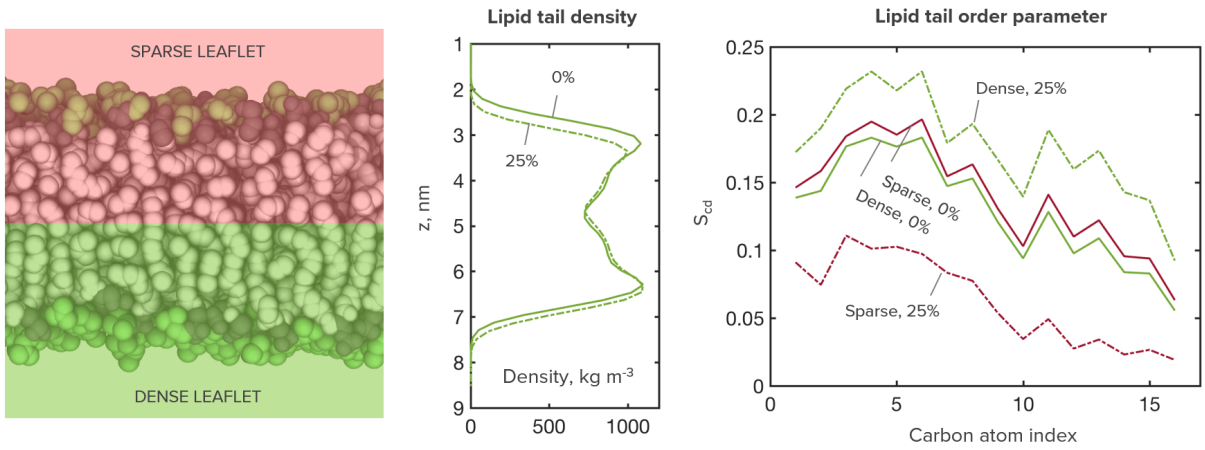

Figure 5. Structural analysis of bilayer with 25% asymmetry compared to symmetric bilayer: (a) snapshot of bilayer structure, (b) density profile along bilayer normal, and (c) deuterium order parameter for each carbon atom in lipid tails.

3.1.2 Frequency of membrane hydrophobic defects

The occurrence of hydrophobic packing defects was analyzed based on 600-ns unbiased atomistic simulations. Figure 6 shows the area distribution of packing defects in the minority leaflet of a symmetric bilayer and a bilayer with 25% asymmetry. The sparse leaflet of the asymmetric bilayer exhibited some significantly larger defects, with some larger than 40 Å^2, compared to the symmetric bilayer, which had a maximum defect area of about 25 Å^2. It is important to note that in both cases, the majority of defects are about the same size (<5 Å^2); however, in the sparse leaflet, larger defects become possible and occur less rarely. These large defects represent significant gaps between head groups, allowing more space for tails to protrude with less interference. In combination with the decrease in order parameter, which is associated with increased mobility of the lipid tails, this result suggests that protrusions are more likely in the sparse leaflet than the dense leaflet. It can therefore be concluded that area asymmetry

increases the likelihood of protrusions and hydrophobic packing defects in the sparse leaflet, both of which are strongly associated with improving the uptake of NPs and peptides.

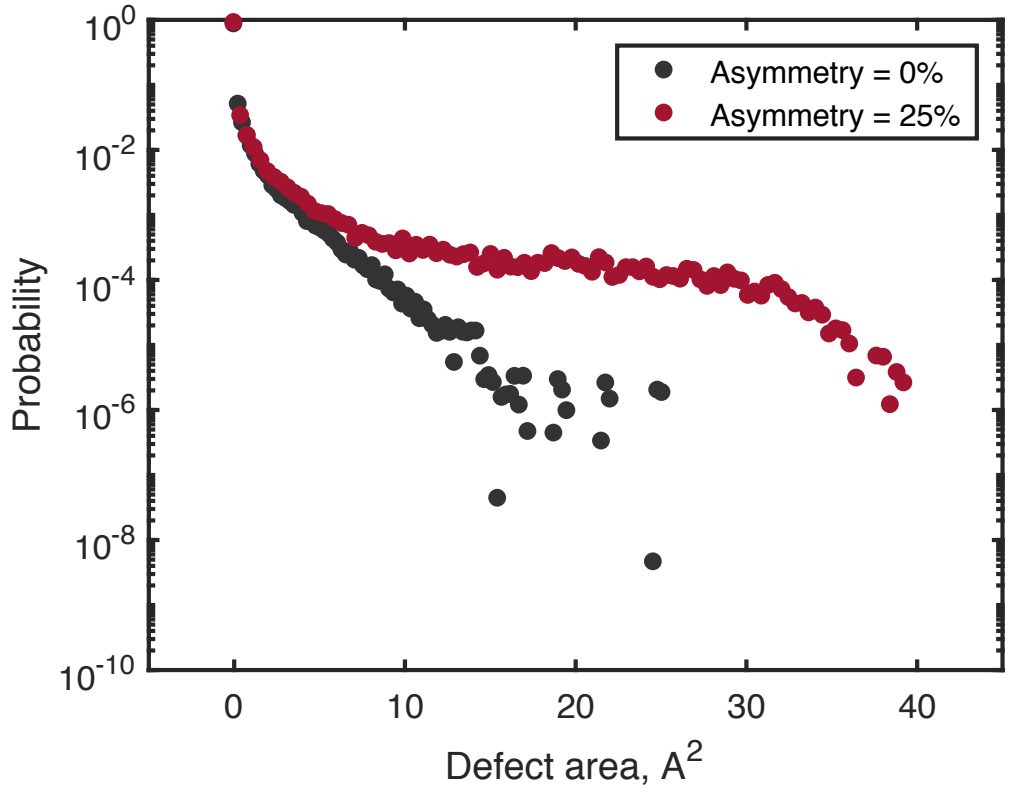

Figure 6. Area distribution of hydrophobic defects for the sparse leaflet of an asymmetric bilayer compared to a leaflet of a symmetric reference bilayer.

3.1.3 Protrusion and desorption potential of mean force

The PMF for producing a splay protrusion was calculated for each leaflet of a membrane with 25% area asymmetry. Based on the PMF profiles shown in Fig. 8, in the hydrophobic core of the bilayer, the energy barrier is small and increases gradually. In this regime, the barrier is mostly due to steric hindrance by neighboring lipid tails, causing protrusions in the dense leaflet

to incur a greater energy cost. When the protrusion begins to interact with water, the energy barrier sharply increases and the PMF enters a second linear regime. Here, as the tail protrudes further away from the bilayer core, the barrier increases at a slope of approximately 28.3 kJ/mol/nm in the dense leaflet and 42.8 kJ/mol/nm in the sparse leaflet. The slope of the PMF for the dense leaflet is similar to that calculated for symmetric DOPC bilayers (27.6 kJ/mol/nm) [11]. At the distance corresponding to $d_p = 0$ from the bilayer center of mass (2.1 nm and 1.8 nm for the dense and sparse leaflets, respectively), the free energy cost was significantly lower in the sparse leaflet (2.6 kJ/mol vs. 27.9 kJ/mol). It was shown previously that the cost a protrusion reaching $d_p = 0$ in a symmetric DOPC bilayer is approximately 20.9 kJ/mol [11], meaning that membrane asymmetry decreases the barrier to protrusions in the minority leaflet while increasing it in the majority leaflet. The increase in slope for the sparse leaflet can thus be explained by the fact that the energy barrier is significantly lower to cross the head group plane but is the same when the lipid is free in solution. This result makes sense based on the structural changes previously discussed, since the decreased density and order parameter and increase in packing defect size allow for protrusions to occur more easily. The PMF thus provides an additional thermodynamic justification for the assertion that protrusion frequency increases in the sparse leaflet as asymmetry increases.

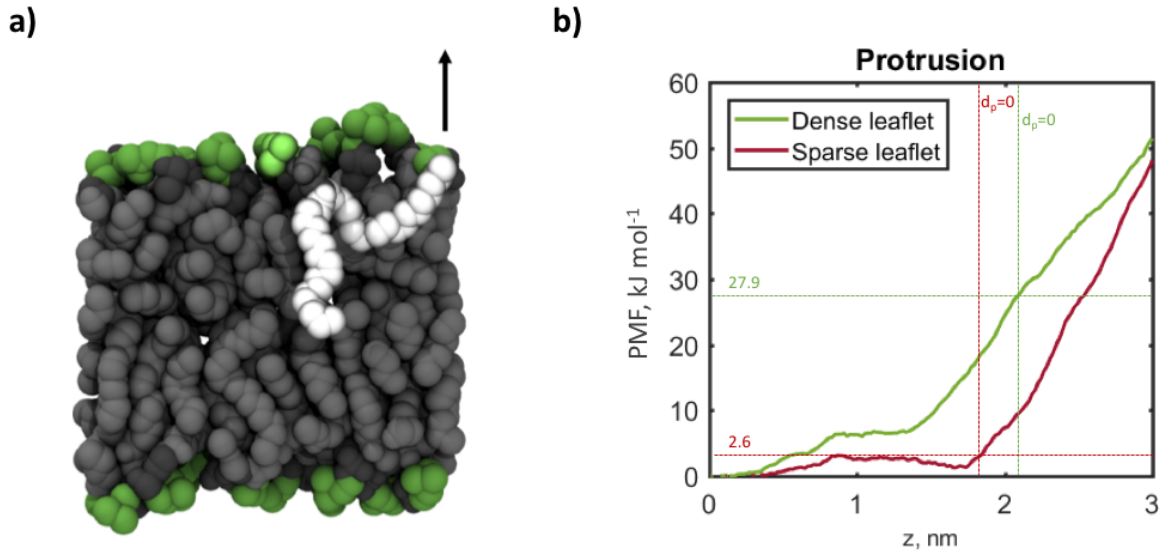

Figure 7. (a) Snapshot and (b) PMF of splay protrusion. Dotted lines represent the average position of phosphate atoms in each leaflet relative to the bilayer center of mass ($d_p = 0$).

In unbiased simulations of asymmetric bilayers in the presence of NPs, lipids were occasionally observed to desorb from the bilayer (specifically the densely-packed leaflet) and attach to the surface of the NP. To determine whether membrane asymmetry affects the likelihood of this occurring, the free energy cost of desorption was calculated for symmetric and 25% asymmetric bilayers. Figure 8 shows the PMF for removing a lipid from each leaflet of the bilayer into the solvent. Within the bilayer, the energy barrier for desorption is greater in the dense leaflet due to the tightly packed lipid tails. However, once the desorbing lipid passes its energy minimum (at the phosphate plane), the two PMFs are very similar because the energy barrier is caused by the unfavorable interactions with water rather than with other lipids. Previous atomistic simulations of dipalmitoyl-phosphatidylcholine (DPPC) bilayers have estimated the cost of desorption in symmetric bilayers to be 60–80 kJ/mol (14–19 kcal/mol) [41], [42], while that of DOPC was slightly higher at 90 kJ/mol (21.5 kcal/mol) [43], and the results here are comparable. In this regime for the sparse leaflet, the magnitude of the energy barrier to

desorption is comparable to that of a protrusion at the same distance, so either or both could occur with similar likelihood. However, in the dense leaflet the barrier for a protrusion is significantly higher than that of desorption. Since the timescale for protrusion and desorption events scales exponentially with the energy barrier, this different is sufficient to conclude that desorption is the dominant defect mode in the dense leaflet.

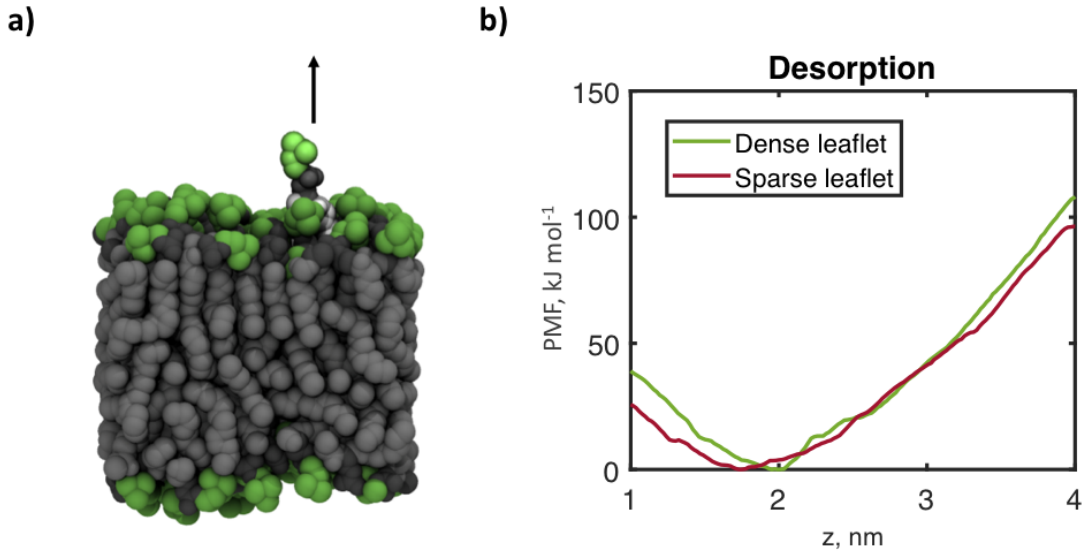

Figure 8. (a) Snapshot and (b) PMF of lipid desorption. Dotted lines represent the average position of phosphate atoms in each leaflet relative to the bilayer center of mass ($d_p = 0$).

3.2 Nanoparticle uptake behavior

3.2.1 Insertion latency

One of the most important factors in the efficacy of NPs for purposes such as drug delivery and protein mimetics is the time it takes a particle to insert into its target membrane when it reaches it. In order to efficiently administer NP treatments, it is necessary to reduce the insertion latency as much as possible. As discussed above, the structural and defect properties of

asymmetric membranes are favorable to NP insertion, particularly in the sparse leaflet due to the increased likelihood of protrusions and hydrophobic packing defects. To assess whether insertion latency is indeed reduced by membrane asymmetry, unbiased simulations of MUS:OT NPs on each leaflet of symmetric and asymmetric membranes were run over long time scales. Figure 9 shows the fraction of NPs inserted as a function of simulation time. This data shows that insertion latency is drastically reduced in asymmetric bilayers, for both leaflets. The number of NPs inserted in the symmetric reference bilayer increased very slowly over time, eventually saturating at only ~30% inserted. On the other hand, both leaflets of the asymmetric bilayer had very high uptake over short times, particularly the sparse leaflet. In the first ~100 ns of simulation, about 20% of the NPs on the sparse leaflet had inserted, compared to less than 15% of those on the dense leaflet and only a single NP in the reference bilayer. The sparse leaflet reached 50% insertion before 1 μm, and the insertion rate in the dense leaflet was similar until that point, when it saturated at just over 45% insertion. The abrupt saturation thresholds are likely due to incomplete sampling; with a larger number of trials the full curves could be established. However, it is clear that introducing area asymmetry in lipid membranes significantly decreases NP insertion latency.

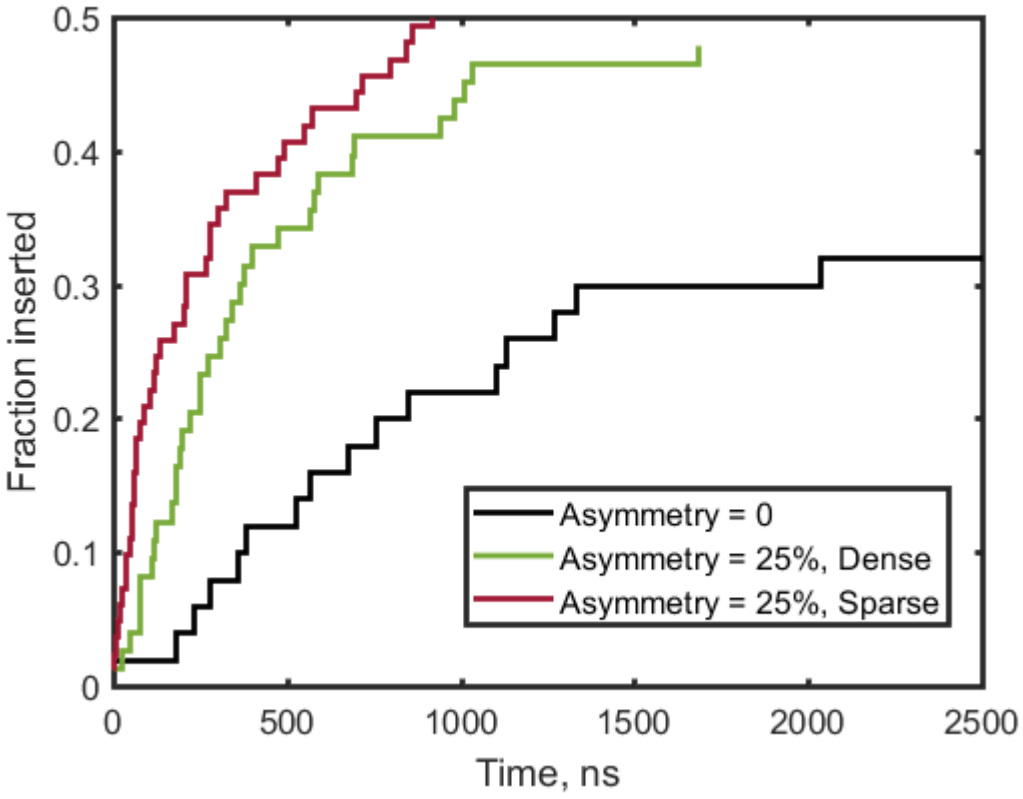

Figure 9. Fraction of NPs inserted as a function of simulation time in dense and sparse leaflets of 25% asymmetric bilayer compared to reference bilayer, showing that insertion latency decreases in both leaflets in asymmetric membranes.

These results are not surprising for the sparse leaflet, but fact that the effect is so strong in the dense leaflet is unexpected and could have important implications for the practical use of AuNPs. It is well established that positive membrane curvature increases the frequency of protrusions and hydrophobic packing defects, which mediate the insertion of NPs and membrane proteins [11], [21], [24]. Negative curvature, on the other hand, suppresses these defects and therefore could be assumed to reduce the likelihood of NP uptake via the established pathways. However, this result suggests that NP insertion may be enhanced even in membranes with negative curvature or tight lipid packing, widening the range of potential targets for treatment.

3.2.2 Transition state analysis

To determine the mechanism by which NP uptake is enhanced by membrane asymmetry, the transition state for insertion in both leaflets of a 25% asymmetric bilayer was identified via committor analysis, as described in Section 2.5. Figure 10 shows the committor p as a function of starting configuration time, between 60 and 70 ns for the sparse leaflet and between 72 and 82 ns for the dense leaflet. As expected, p starts near 0 and ends at 1 in both cases, indicating that the committor calculation was performed correctly. The value of p does not always monotonically increase with time due to the fact that in an unbiased simulation, the particle may fluctuate back and forth on one side of the energy barrier several times before overcoming it. In other words, accessing a state with higher probability of committing to insertion does not necessarily guarantee that the particle will insert directly from that state [21]. The time of the transition state $p = 0.5$ was calculated by interpolation to be 76.7 ns for the dense leaflet and 64.16 ns for the sparse leaflet.

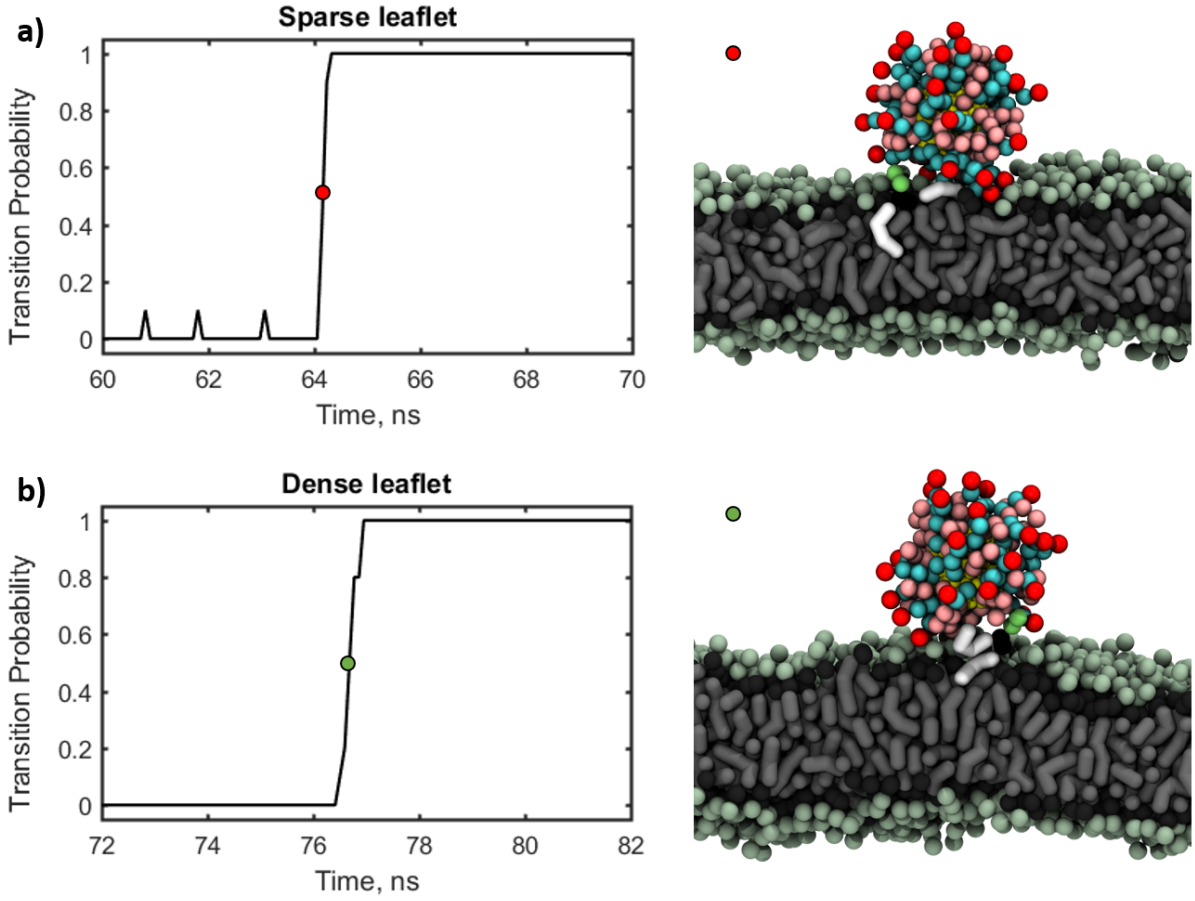

Figure 10. On the left are lots of the committor, p, as a function of starting configuration time, where the red and green dots indicate the interpolated times of the transition state ($p = 0.5$), and on the right are snapshots of the transition state for (a) the sparse leaflet and (b) the dense leaflet.

The configurations corresponding to these transition states are also shown in Fig. 10 to the right of the committor plots. These snapshots clearly show that the uptake mechanism was very different between the two leaflets. In the sparse leaflet, insertion was mediated by contact between a protruding lipid tail in the solvent and a hydrophobic ligand of the NP. This initial contact was quickly followed by the protruding tail shielding itself from water by embedding itself within the NP monolayer, pulling the NP closer to the membrane core and triggering contact with other lipid tails, effectively making it more energetically favorable for the particle to

bury itself in the bilayer core than remain in the solvent. This mechanism makes sense based on the structural and energetic characteristics of the sparse leaflet discussed above, as well as previous studies of protrusion-mediated NP uptake [21], [22]. Based on the snapshot shown in Fig. 10(a), this transition state is also associated with the NP moving into close contact with the surface of the bilayer, an effect that may be due to the increased accessible area between heads.

The transition state for the dense leaflet was characterized by a very different phenomenon. Here, a lipid atom desorbs from the bilayer close to the NP and attaches to the hydrophobic regions of the NP monolayer. This event catalyzes the desorption of several more lipids which adsorb to the surface of the NP, causing the NP to nestle within the dense leaflet. This behavior can be explained by the fact that as discussed previously, the energy cost of desorption from the dense leaflet is significantly less than that of a protrusion. These results suggest that while both protrusion and desorption are both potential modes of insertion in the sparse leaflet, lipids are densely packed the dominant pathway by which amphiphilic NPs insert is solely desorption-mediated. To the best of our knowledge, this is the first time that a desorption-mediated mechanism has been reported for NP uptake by lipid membranes, therefore presenting a novel insertion pathway for particles into densely packed leaflets.

Unlike protrusion-mediated insertion, this mechanism does not result in the NP immediately adopting a symmetric transmembrane configuration, with the particle instead becoming surrounded by desorbed lipids (see Fig. 11). In this state, the membrane near the NP is drastically perturbed. We propose that the NP begins to fully insert from this configuration when the membrane asymmetry relaxes, resulting in the same final state for both leaflets. Before obtaining the final symmetric configuration, the NP passes through an asymmetrically inserted state where it is embedded in only one leaflet and the ligands have not fully flipped to the other

side of the membrane [3], [22]. Eventually, when half the ligands have flipped across the membrane, the particle reaches its final stable configuration. Figure 11 shows the proposed generalized insertion pathway for the dense and sparse leaflet. It is important to note that these transition states were derived from only one insertion trajectory for each leaflet. In reality, there are many possible state trajectories a particle may take between states A and B. Each of these trajectories has at least one transition state, which may correspond to one or more insertion mechanisms. Therefore, for a fuller picture, transition states should be identified for several different trajectories to produce a transition state ensemble [44]. However, the transition states identified above are likely to represent the dominant insertion modes due to their agreement with the structural and thermodynamic properties of leaflets in asymmetric membranes.

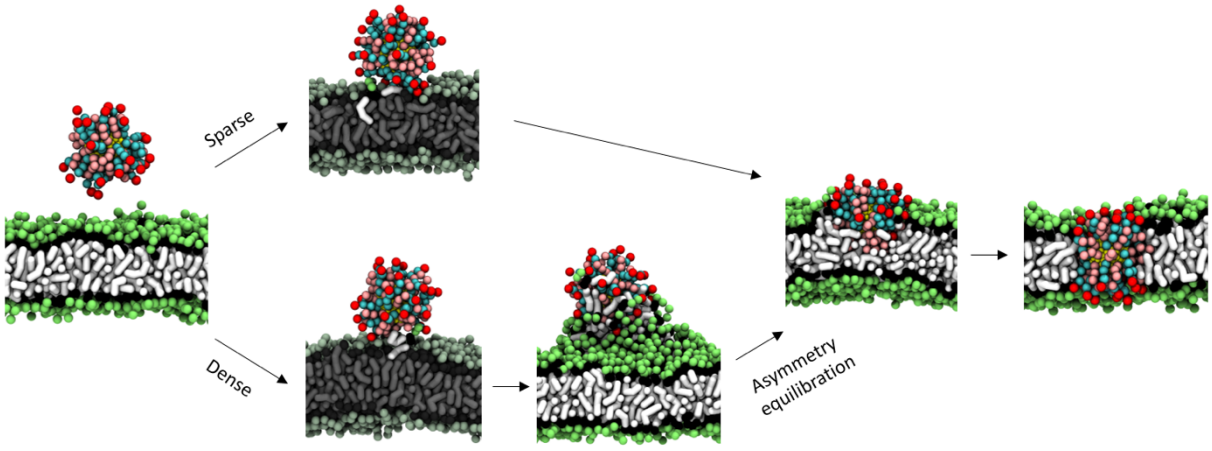

Figure 11. Proposed pathways for insertion into dense and sparse leaflets of an asymmetric membrane, where insertion is mediated by protrusion and desorption, respectively. In the desorption-mediated pathway, a full symmetrically inserted configuration is not obtained until the membrane asymmetry relaxes, until which the NP is fixed to the surface of the bilayer by desorbed lipids.

3.3 Effect of tension on membrane-nanoparticle interactions

3.3.1 Bilayer structural characteristics

Bilayer tension caused by lateral forces is another common structural perturbation in biological membranes which occurs during situations such as osmotic expansion. It is therefore important to understand how the interactions of NPs with bilayer membranes changes under lateral tension. To this end, tension was incrementally applied to bilayers with and without an NP embedded in the center. The box size in the equilibrated, untensed state was approximately 10 nm. As the box size increased by 0.2 nm at each equilibration stage, the bilayer became thinner and the lipids began to spread out horizontally; the thickness of the bilayer decreased from approximately 3.8 nm in an untensed state to approximately 2.0 nm immediately before rupture, a reduction of almost 50%. The charged lipid head groups also tended to aggregate as the membrane expanded, leaving large contiguous regions of hydrophobic defects between them.

The density profiles along the bilayer normal and the order parameters of each carbon in the tail were also measured for tensed and untensed membranes. In agreement with observations, the density significantly decreased as the tension on the membrane increases and the thickness decreases (Fig. 12(a)). The lipids also became significantly more disordered across the entire tail chain as the density decreased because the tail atoms had more configurational freedom. As shown in Fig. 12(b), the order parameter for the tensed membrane drops slightly below zero due to incomplete sampling; this is not entirely physical since S_{CD} should be between 0 and 0.5, but nonetheless it reflects an extremely low ordering in the tense membrane. This result also agrees with previous simulation and experimental studies which have shown that bilayer fluidity (as determined by order parameters and lipid diffusion coefficients) increases significantly under tension [45]. It also in accordance with the trend found in asymmetric membranes as area per

lipid increases, suggesting a potential connection between membrane tension and the likelihood of NP insertion. Moreover, mechanical stress on lipid membranes is known to trigger conformational changes in membrane proteins [46], so it is likely to have a similar effect on embedded NPs.

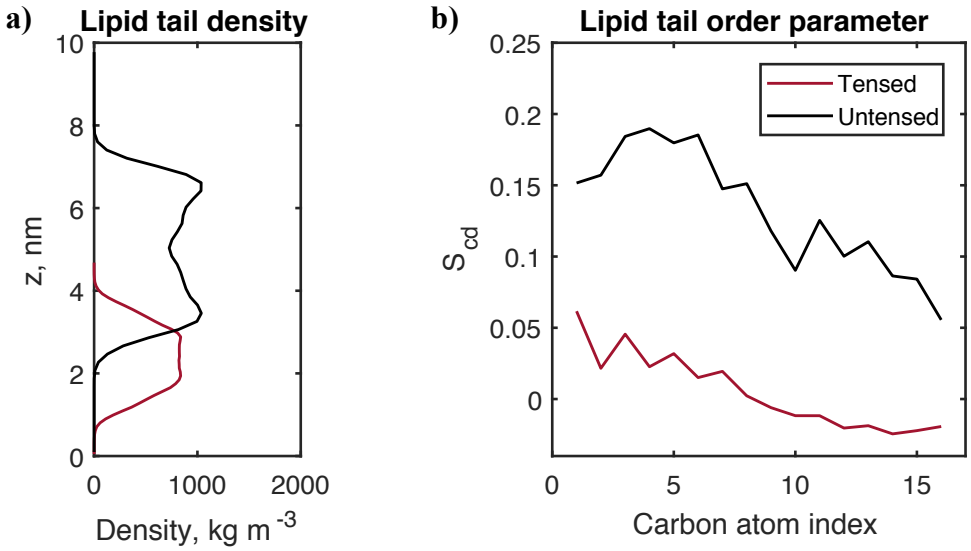

Figure 12. Structural characteristics of tensed and untensed membranes: (a) density profiles and (b) deuterium order parameters.

3.3.2 Membrane-nanoparticle interactions under tension

With no NP present, the bilayer maintained its shape up to 14.6 nm, after which (at 48% total expansion) a large pore formed in the membrane and continued to expand. The presence of an embedded NP decreased the bilayer's resistance to tension, with poration beginning at a box size of 14.2 nm (42% total expansion). Interestingly, here the initial rupture occurred at the location of some of the MUS ligands, whereas it occurred in the corner of the box when no NP was present (Fig. 13). Given that the rupture location is expected to be random in pure lipid

bilayers, it is unknown whether the NP directly caused the rupture; therefore, more trials will be needed to demonstrate robustness in this behavior. However, the decrease in failure threshold shows that the structural integrity of the bilayer under tension is affected by the behavior of the NP, and the difference in failure mode suggests that the rupture mechanism is related to the behavior of the ligands under tension.

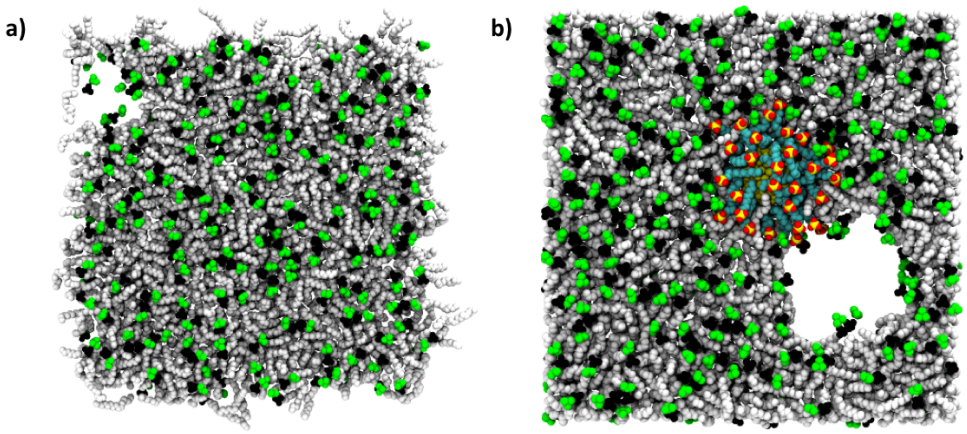

Figure 13. Difference in membrane failure mode in (a) a pure DOPC bilayer and (b) a bilayer with embedded NP. The two bilayers ruptured at 48% and 42% expansion, respectively.

One explanation is that lateral tension affects the probability of a ligand moving through the hydrophobic region of the bilayer, disrupting the membrane structure and initiating rupture. As described previously, nanoparticles embedded in bilayer membranes adopt an energy-minimizing snorkeling configuration in which the charged ligands separate to the polar interfaces on either side of the bilayer. However, occasionally a ligand may "flip" from one leaflet to the other, changing the configuration of the NP and transiently affecting the local membrane structure. Based on the drastic changes in density and order parameter described above, the ligand flipping barrier is expected to significantly decrease under tension because the increased

space and mobility of the lipid tails allows the surrounding lipids to accommodate the movement of a ligand. The flipping of embedded ligands across the membrane has not previously been reported; however, the decreased ligand flipping barrier could also impact the initial uptake of amphiphilic NPs into the membrane. Previous studies have suggested that the nondisruptive transition between being adsorbed on the surface to being fully embedded may proceed by iteratively flipping ligands one-by-one across the bilayer until the NP is in a fully snorkeled state [3], [47]. Therefore, the reduction in ligand flipping barrier and increase in accessible hydrophobic areas suggest that lateral tension may be an additional mechanism by which insertion latency could be reduced in NP-membrane systems.

4. Conclusions and Future Work

This thesis explored the interactions between amphiphilic gold nanoparticles and membranes in the presence of structural perturbations such as area asymmetry and lateral tension. Area asymmetry between leaflets was shown to affect bilayer properties such as density, order parameter, and frequency of membrane defects. In particular, lipid tail protrusions and hydrophobic packing defects are known to affect the insertion behavior of nanoparticles. Based on frequency of occurrence and potential of mean force analysis, the likelihood of these defects was shown to increase as area per lipid increased. In general, the similar behavior of asymmetric membranes to that of membranes under other perturbations such as membrane curvature imply that membrane asymmetry could be used as a simple and reproducible proxy for such systems, which can be very difficult and expensive to simulate [24].

Membrane asymmetry was also found to significantly decrease the latency for insertion of NPs into both dense and sparse leaflets. Transition state analysis showed that the dominant

uptake pathway in the sparse leaflet was lipid tail protrusions. The dominant pathway in the dense leaflet was found to be lipid desorption, a novel result that could have important implications for NP deployment strategies. These findings also open many avenues for future investigation. For example, the transition state analysis can be expanded from a single trajectory to a transition state ensemble to determine any other possible insertion pathways.

Finally, lateral tension was shown to produce similar structural perturbations as membrane asymmetry, particularly with respect to order parameter and packing defect areas. The presence of an embedded MUS NP resulted in a decrease in tensile strength and a change in failure mode, where failure occurred at the location of some NP ligands. Tension was also shown to change the structural characteristics of the bilayer so as to decrease the barrier to ligand flipping, which could be a causal factor in spontaneous poration and rupture.

There are many directions for further research on the impact of lateral tension and its relationship with area asymmetry. In this research, lateral tension was modeled in planar bilayer membranes under the assumption that this is a reasonable approximation for local perturbations in larger cellular systems. However, many systems that undergo events such as osmotic shock are small vesicles which may exhibit different behavior due to the higher degree of membrane curvature. Moving forward, this problem can be addressed by simulating the pressure in actual vesicle systems, a problem which was computationally too challenging for the scope of this thesis. In addition, the hypothesis that lateral tension may decrease NP insertion latency due to the decreased ligand flipping barrier should be tested by PMF calculations and by unbiased NP insertion trials. It would also be interesting to apply lateral tension to asymmetric membranes to investigate whether this decreases the insertion latency even further. In summary, this thesis proposes several mechanisms by which NP insertion latency may be reduced in lipid membranes,

which could improve efficiency and efficacy in target drug delivery, imaging, and protein mimetics.

5. References

[1] D. W. Deamer and J. Bramhall, "Permeability of lipid bilayers to water and ionic solutes," *Chem. Phys. Lipids*, vol. 40, no. 2, pp. 167–188, Jun. 1986.

[2] M. A. Wilson and A. Pohorille, "Mechanism of Unassisted Ion Transport across Membrane Bilayers," *J. Am. Chem. Soc.*, vol. 118, no. 28, pp. 6580–6587, Jan. 1996.

[3] R. C. Van Lehn and A. Alexander-Katz, "Grafting Charged Species to Membrane-Embedded Scaffolds Dramatically Increases the Rate of Bilayer Flipping," *ACS Cent. Sci.*, vol. 3, no. 3, pp. 186–195, Mar. 2017.

[4] E. Gouaux and R. Mackinnon, "Principles of selective ion transport in channels and pumps," *Science*, vol. 310, no. 5753, pp. 1461–1465, Dec. 2005.

[5] D. J. Lockhart and P. S. Kim, "Internal stark effect measurement of the electric field at the amino terminus of an alpha helix," *Science*, vol. 257, no. 5072, pp. 947–951, Aug. 1992.

[6] M. Suzuki, T. Morita, and T. Iwamoto, "Diversity of Cl(-) channels," *Cell. Mol. Life Sci. CMLS*, vol. 63, no. 1, pp. 12–24, Jan. 2006.

[7] M. J. Welsh, "Abnormal regulation of ion channels in cystic fibrosis epithelia," *FASEB J. Off. Publ. Fed. Am. Soc. Exp. Biol.*, vol. 4, no. 10, pp. 2718–2725, Jul. 1990.

[8] C. A. Hübner and T. J. Jentsch, "Ion channel diseases," *Hum. Mol. Genet.*, vol. 11, no. 20, pp. 2435–2445, Oct. 2002.

[9] N. A. Shirwany, D. Payette, J. Xie, and Q. Guo, "The amyloid beta ion channel hypothesis of Alzheimer's disease," *Neuropsychiatr. Dis. Treat.*, vol. 3, no. 5, pp. 597–612, 2007.

[10] L. V. Chernomordik and M. M. Kozlov, "Protein-Lipid Interplay in Fusion and Fission of Biological Membranes," *Annu. Rev. Biochem.*, vol. 72, no. 1, pp. 175–207, 2003.

[11] M. A. Tahir, R. C. Van Lehn, S. H. Choi, and A. Alexander-Katz, "Solvent-exposed lipid tail protrusions depend on lipid membrane composition and curvature," *Biochim. Biophys. Acta BBA - Biomembr.*, vol. 1858, no. 6, pp. 1207–1215, Jun. 2016.

[12] M. Ferrari, "Cancer nanotechnology: opportunities and challenges," *Nat. Rev. Cancer*, vol. 5, no. 3, pp. 161–171, Mar. 2005.

[13] M. E. Davis, Z. (Georgia) Chen, and D. M. Shin, "Nanoparticle therapeutics: an emerging treatment modality for cancer," *Nat. Rev. Drug Discov.*, vol. 7, no. 9, pp. 771–782, Sep. 2008.

[14] P. Ghosh, G. Han, M. De, C. K. Kim, and V. M. Rotello, "Gold nanoparticles in delivery applications," *Adv. Drug Deliv. Rev.*, vol. 60, no. 11, pp. 1307–1315, Aug. 2008.

[15] L. M. Bareford and P. W. Swaan, "Endocytic mechanisms for targeted drug delivery," *Adv. Drug Deliv. Rev.*, vol. 59, no. 8, pp. 748–758, Aug. 2007.

[16] J. Chen *et al.*, "Cationic Nanoparticles Induce Nanoscale Disruption in Living Cell Plasma Membranes," *J. Phys. Chem. B*, vol. 113, no. 32, pp. 11179–11185, Aug. 2009.

[17] R. C. Van Lehn *et al.*, "Effect of Particle Diameter and Surface Composition on the Spontaneous Fusion of Monolayer-Protected Gold Nanoparticles with Lipid Bilayers," *Nano Lett.*, vol. 13, no. 9, pp. 4060–4067, Sep. 2013.

[18] E. Strandberg and J. A. Killian, "Snorkeling of lysine side chains in transmembrane helices: how easy can it get?," *FEBS Lett.*, vol. 544, no. 1, pp. 69–73, Jun. 2003.

[19] R. C. V. Lehn and A. Alexander-Katz, "Penetration of lipid bilayers by nanoparticles with environmentally-responsive surfaces: simulations and theory," *Soft Matter*, vol. 7, no. 24, pp. 11392–11404, Nov. 2011.

[20] R. C. Van Lehn and A. Alexander-Katz, "Membrane-Embedded Nanoparticles Induce Lipid Rearrangements Similar to Those Exhibited by Biological Membrane Proteins," *J. Phys. Chem. B*, vol. 118, no. 44, pp. 12586–12598, Nov. 2014.
[21] R. C. V. Lehn *et al.*, "Lipid tail protrusions mediate the insertion of nanoparticles into model cell membranes," *Nat. Commun.*, vol. 5, p. 4482, Jul. 2014.
[22] R. C. V. Lehn and A. Alexander-Katz, "Pathway for insertion of amphiphilic nanoparticles into defect-free lipid bilayers from atomistic molecular dynamics simulations," *Soft Matter*, vol. 11, no. 16, pp. 3165–3175, Apr. 2015.
[23] S. Vanni *et al.*, "Amphipathic lipid packing sensor motifs: probing bilayer defects with hydrophobic residues," *Biophys. J.*, vol. 104, no. 3, pp. 575–584, Feb. 2013.
[24] L. Vamparys *et al.*, "Conical lipids in flat bilayers induce packing defects similar to that induced by positive curvature," *Biophys. J.*, vol. 104, no. 3, pp. 585–593, Feb. 2013.
[25] H. Heerklotz, "Membrane Stress and Permeabilization Induced by Asymmetric Incorporation of Compounds," *Biophys. J.*, vol. 81, no. 1, pp. 184–195, Jul. 2001.
[26] S. Esteban-Martín, H. J. Risselada, J. Salgado, and S. J. Marrink, "Stability of Asymmetric Lipid Bilayers Assessed by Molecular Dynamics Simulations," *J. Am. Chem. Soc.*, vol. 131, no. 42, pp. 15194–15202, Oct. 2009.
[27] E. S. Haswell, R. Phillips, and D. C. Rees, "Mechanosensitive channels: what can they do and how do they do it?," *Struct. Lond. Engl. 1993*, vol. 19, no. 10, pp. 1356–1369, Oct. 2011.
[28] M. Louhivuori, H. J. Risselada, E. van der Giessen, and S. J. Marrink, "Release of content through mechano-sensitive gates in pressurized liposomes," *Proc. Natl. Acad. Sci.*, vol. 107, no. 46, pp. 19856–19860, Nov. 2010.
[29] J. Y. Xie, G. H. Ding, and M. Karttunen, "Molecular dynamics simulations of lipid membranes with lateral force: Rupture and dynamic properties," *Biochim. Biophys. Acta BBA - Biomembr.*, vol. 1838, no. 3, pp. 994–1002, Mar. 2014.
[30] K. Lai, B. Wang, Y. Zhang, and Y. Zheng, "Computer simulation study of nanoparticle interaction with a lipid membrane under mechanical stress," *Phys. Chem. Chem. Phys.*, vol. 15, no. 1, pp. 270–278, Dec. 2012.
[31] B. J. Alder and T. E. Wainwright, "Studies in Molecular Dynamics. I. General Method," *J. Chem. Phys.*, vol. 31, no. 2, pp. 459–466, Aug. 1959.
[32] J. Wildman, P. Repiščák, M. J. Paterson, and I. Galbraith, "General Force-Field Parametrization Scheme for Molecular Dynamics Simulations of Conjugated Materials in Solution," *J. Chem. Theory Comput.*, vol. 12, no. 8, pp. 3813–3824, Aug. 2016.
[33] C. Oostenbrink, A. Villa, A. E. Mark, and W. F. V. Gunsteren, "A biomolecular force field based on the free enthalpy of hydration and solvation: The GROMOS force-field parameter sets 53A5 and 53A6," *J. Comput. Chem.*, vol. 25, no. 13, pp. 1656–1676, Oct. 2004.
[34] J. Barnoud and L. Monticelli, "Coarse-Grained Force Fields for Molecular Simulations," in *Molecular Modeling of Proteins*, Humana Press, New York, NY, 2015, pp. 125–149.
[35] B. Hess, C. Kutzner, D. van der Spoel, and E. Lindahl, "GROMACS 4: Algorithms for Highly Efficient, Load-Balanced, and Scalable Molecular Simulation," *J. Chem. Theory Comput.*, vol. 4, no. 3, pp. 435–447, Mar. 2008.
[36] N. Schmid *et al.*, "Definition and testing of the GROMOS force-field versions 54A7 and 54B7," *Eur. Biophys. J.*, vol. 40, no. 7, p. 843, Jul. 2011.
[37] B. Hess, "P-LINCS: A Parallel Linear Constraint Solver for Molecular Simulation," *J. Chem. Theory Comput.*, vol. 4, no. 1, pp. 116–122, Jan. 2008.

[38] W. Humphrey, A. Dalke, and K. Schulten, “VMD: Visual molecular dynamics,” *J. Mol. Graph.*, vol. 14, no. 1, pp. 33–38, Feb. 1996.
[39] S. Kumar, J. M. Rosenberg, D. Bouzida, R. H. Swendsen, and P. A. Kollman, “THE weighted histogram analysis method for free-energy calculations on biomolecules. I. The method,” *J. Comput. Chem.*, vol. 13, no. 8, pp. 1011–1021, Oct. 1992.
[40] L. S. Vermeer, B. L. de Groot, V. Réat, A. Milon, and J. Czaplicki, “Acyl chain order parameter profiles in phospholipid bilayers: computation from molecular dynamics simulations and comparison with 2H NMR experiments,” *Eur. Biophys. J.*, vol. 36, no. 8, pp. 919–931, Nov. 2007.
[41] D. P. Tieleman and S.-J. Marrink, “Lipids Out of Equilibrium: Energetics of Desorption and Pore Mediated Flip-Flop,” *J. Am. Chem. Soc.*, vol. 128, no. 38, pp. 12462–12467, Sep. 2006.
[42] A. Grafmüller, R. Lipowsky, and V. Knecht, “Effect of tension and curvature on the chemical potential of lipids in lipid aggregates,” *Phys. Chem. Chem. Phys.*, vol. 15, no. 3, pp. 876–881, Dec. 2012.
[43] N. Sapay, W. F. D. Bennett, and D. P. Tieleman, “Thermodynamics of flip-flop and desorption for a systematic series of phosphatidylcholine lipids,” *Soft Matter*, vol. 5, no. 17, pp. 3295–3302, Aug. 2009.
[44] R. Du, V. S. Pande, A. Y. Grosberg, T. Tanaka, and E. S. Shakhnovich, “On the transition coordinate for protein folding,” *J. Chem. Phys.*, vol. 108, no. 1, pp. 334–350, Jan. 1998.
[45] A. S. Reddy, D. T. Warshaviak, and M. Chachisvilis, “Effect of membrane tension on the physical properties of DOPC lipid bilayer membrane,” *Biochim. Biophys. Acta*, vol. 1818, no. 9, pp. 2271–2281, Sep. 2012.
[46] A. G. Lee, “How lipids affect the activities of integral membrane proteins,” *Biochim. Biophys. Acta BBA - Biomembr.*, vol. 1666, no. 1, pp. 62–87, Nov. 2004.
[47] F. Simonelli, D. Bochicchio, R. Ferrando, and G. Rossi, “Monolayer-Protected Anionic Au Nanoparticles Walk into Lipid Membranes Step by Step,” *J. Phys. Chem. Lett.*, vol. 6, no. 16, pp. 3175–3179, Aug. 2015.